OXFORD

Structural bioinformatics

Effective drug–target interaction prediction with mutual interaction neural network

Fei Li [ORCID] **[1], Ziqiao Zhang[1], Jihong Guan[2] and Shuigeng Zhou** [ORCID] **[1,3,*]**

[1]School of Computer Science, Fudan University, Shanghai 200438, China, [2]Department of Computer Science and Technology, Tongji University, Shanghai 201804, China and [3]Shanghai Key Lab of Intelligent Information Processing, Shanghai 200438, China

*To whom correspondence should be addressed.

Associate Editor: Pier Luigi Martelli

Abstract

Motivation: Accurately predicting *drug–target interaction* (DTI) is a crucial step to drug discovery. Recently, deep learning techniques have been widely used for DTI prediction and achieved significant performance improvement. One challenge in building deep learning models for DTI prediction is how to appropriately represent drugs and targets. Target distance map and molecular graph are low dimensional and informative representations, which however have not been jointly used in DTI prediction. Another challenge is how to effectively model the mutual impact between drugs and targets. Though attention mechanism has been used to capture the one-way impact of targets on drugs or vice versa, the mutual impact between drugs and targets has not yet been explored, which is very important in predicting their interactions.

Results: Therefore, in this article we propose MINN-DTI, a new model for DTI prediction. MINN-DTI combines an interacting-transformer module (called Interformer) with an improved Communicative Message Passing Neural Network (CMPNN) (called Inter-CMPNN) to better capture the two-way impact between drugs and targets, which are represented by molecular graph and distance map, respectively. The proposed method obtains better performance than the state-of-the-art methods on three benchmark datasets: DUD-E, human and BindingDB. MINN-DTI also provides good interpretability by assigning larger weights to the amino acids and atoms that contribute more to the interactions between drugs and targets.

Availability and implementation: The data and code of this study are available at https://github.com/admislf/MINN-DTI.

Contact: sgzhou@fudan.edu.cn

1 Introduction

In drug discovery and design, verifying whether a drug interacts with a certain target is a key step to prove the effectiveness of the drug. Since large-scale *in vitro* and *in vivo* experiments are high-cost and time consuming, computational methods for *drug–target interaction* (DTI in short) prediction have received increasing attention. However, traditional computational methods have obvious limitations. For example, the widely used molecular docking is inefficient and sometimes ineffective because of its huge amount of computation and inaccurate scoring function (Su *et al.*, 2019). On the other hand, traditional machine learning models such as Random Forest (RF) and Support Vector Machine (SVM) have also been used for DTI prediction (Ballester and Mitchell, 2010; Bleakley and Yamanishi, 2009; Liu *et al.*, 2015). These methods are generally simple and efficient, but the performance is far from satisfaction. Recently, the introduction of deep learning models to DTI prediction has greatly advanced this area (Bagherian *et al.*, 2021;

Tian *et al.*, 2016). In deep learning-based works, DTI prediction can be characterized as a binary classification, a ranking task or a regression task for binding affinity. Usually, deep learning models for DTI prediction are composed of a target feature extraction module, a drug feature extraction module and a prediction module. These modules are carefully designed according to various practical factors including the input representations.

The most commonly used representations of drugs and targets are one-dimensional (1D) sequences such as Simplified Molecular Input Line Entry Specification (SMILES) strings for drugs and amino acid sequences for targets (Karimi *et al.*, 2019; Liu *et al.*, 2020; Peng *et al.*, 2020; Tsubaki *et al.*, 2019; Zheng *et al.*, 2020). The models with 1D sequences as input generally use Convolutional Neural network (CNN), Recurrent Neural Network (RNN), Long Short-Term Memory (LSTM) blocks or Gated Recurrent Unit (GRU) blocks to extract drug and target features. For instance, Ozturk *et al.* used CNN modules to extract hidden representations of amino acid sequences and SMILES strings, which were later combined and

input to a multi-layer perceptron to perform the prediction (Ozturk *et al.*, 2018). Besides sequences, feature vectors representing physicochemical properties of targets/drugs and drug molecular fingerprints are also common forms of 1D input to DTI prediction models (Lee *et al.*, 2019; Lenselink *et al.*, 2017; Rifaioglu *et al.*, 2021). Slightly different from the work of Ozturk *et al.*, instead of SMILES strings, Lee *et al.* used molecular fingerprints with fully connected networks to extract drug features to predict DTI prediction (Lee *et al.*, 2019). According to the research of Lenselink et al. (2017), with feature vectors composed of physicochemical properties of targets/drugs and molecular fingerprints as input, Deep Neural Network (DNN) models outperform Naive Bayes, RF, SVM, logistic regression models in DTI prediction. Two-dimensional (2D) paired feature map has also been used for DTI prediction, which uses a matrix of a specific property calculated for amino acid pairs in the corresponding protein sequence to represent a target (Rifaioglu *et al.*, 2021; Zheng *et al.*, 2020). For example, Rifaioglu *et al.* used multichannel protein feature maps involving sequence, structural, evolutionary and physicochemical properties to represent proteins for proteochemometric protein-drug binding affinity prediction (Rifaioglu *et al.*, 2021). 2D structural images are intuitive representations of drugs and have been used in DTI prediction (Rifaioglu *et al.*, 2020; Wang *et al.*, 2021). Wang *et al.* proposed an efficient DTI prediction system using only 2D images as input, which includes CNN-based models for 704 targets (Rifaioglu *et al.*, 2020). Two-dimensional (2D) molecular graph is another effective representation of drugs, which has been widely used in Graph Neural Network (GNN)-based models for predicting molecular properties (Gilmer *et al.*, 2017; Song *et al.*, 2020; Xiong *et al.*, 2020; Yang *et al.*, 2019; Zhang *et al.*, 2021). Recently, molecular graph has also been increasingly used in DTI prediction (Nguyen *et al.*, 2021; Torng and Altman, 2019; Tsubaki *et al.*, 2019). Tsubaki *et al.* used GNN to extract the information of a small molecule as a feature vector, which is then concatenated with the target feature vector extracted by CNN from amino acid sequence to make prediction (Tsubaki *et al.*, 2019). Compared with SMILES-based models, graph-based models can readily exploit topological information of molecules, which show obvious advantages in the task of DTI prediction.

Although 1D and 2D-based DTI prediction models have made significant progress recently, as DTI is in essence three-dimensional (3D) physical interaction, so it is natural and reasonable to predict DTI using three-dimensional structural information. Many studies directly use 3D Cartesian coordinates to represent the 3D structures of targets, but the limited samples cannot cover such a huge space, which leads to poor performance (Ragoza *et al.*, 2017; Wallach *et al.*, 2015; Zheng *et al.*, 2019). Some models apply 3D voxel grids to represent targets and use 3D-CNN to extract target features, their accuracy is limited because the grid coordinates are not accurate enough to represent the spatial positions of targets' atoms. On the other hand, 2D paired distance map represents 3D structure of each target by a matrix of internal pairwise distances between the amino acids of the target, which has been mainly used in protein structure prediction (Skolnick *et al.*, 1997). Recently, Zheng *et al.* proposed an advanced model called drugVQA to predict DTI, where LSTM and dynamic 2D-CNN were used to extract features from SMILES strings and distance maps, respectively (Zheng *et al.*, 2020), and achieved satisfactory performance. Though 2D paired distance map and molecular graph are promising representations of targets and drugs, respectively. However, they have not yet been jointly used for DTI prediction.

After extracting feature vectors from the drug and the target, respectively, the features are usually concatenated and input to a MLP to predict DTI. In most existing models, targets and drugs are represented and processed separately, they can hardly capture the interacting context between targets and drug molecules. The attention mechanism is often used to acquire the contributions of different components of a drug or target to the interaction (Karimi *et al.*, 2019; Tsubaki *et al.*, 2019; Zheng *et al.*, 2020), which has been recently used to characterize the interactions between targets and drugs (Chen *et al.*, 2020, 2021). The attention mechanism was found to be able to better capture the impact of targets on drugs and vice versa, so as to obtain better representations. However, these models pay attention only to the impact of one participant of a DTI on the counterpart, such as target on drug, but ignore the reverse impact. According to the induced-fit theory (Johnson, 2008), interacting drug molecules and targets are mutually impacted. Therefore, it is natural and reasonable to consider their mutual impacts when learning to represent the drugs and targets for DTI prediction.

In this article, to overcome the above-mentioned drawbacks of existing DTI prediction models, we propose a new model for DTI prediction. In this model, 2D paired distance maps of proteins and molecular graphs are served as inputs for targets and drugs, respectively. To capture the interactive impacts between targets and drugs, we design a mutual interaction neural network (MINN) by innovatively combining two interacting-transformers (Interformer in short) with an improved Communicative Message Passing Neural Network (CMPNN) (called Inter-CMPNN). In the experiments, our model achieves better performance than state-of-the-art methods on DUD-E, human and BindingDB benchmark datasets. Case studies show that individual contributions of residues in the target and atoms in the drug to the formation of DTI can be inferred from learned attention weights, which indicates that our proposed model is interpretable and can help to explain the drug action mechanism, and suggests the direction of drug optimization in the future.

2 Materials and methods

2.1 Overview

The architecture of our proposed model MINN-DTI is shown in Figure 1. It consists of three modules: a target preprocessing network (TPN), a MINN and an interaction prediction network (IPN). MINN is the core component of our model, which consists of an Interformer module and an Inter-CMPNN module. The Interformer module is constructed by two interacting transformer decoders, and the Inter-CMPNN module is a variant of CMPNN. With these two modules, we can extract the latent vectors of targets and drugs while considering their interacting contexts.

The 2D distance map and 2D molecular graph are served as the input representation of a given target and a molecule, respectively. The molecular graph is directly used, while the distance map is firstly preprocessed by the target preprocessing network (TPN). The latent feature vectors of both the target and the molecule are extracted by MINN. These latent feature vectors are then concatenated and fed to the interaction prediction network (IPN) to predict DTI. The details of these modules are presented in the following sections.

2.2 Target preprocessing network

Given a target, we calculate a 2D paired distance map (Skolnick *et al.*, 1997), which is subsequently preprocessed by the target preprocessing network (TPN) into a fixed-size matrix following drugVQA (Zheng *et al.*, 2020). TPN is implemented by a dynamic attentive CNN. As shown in Figure 2, the dynamic attentive CNN is composed of a Dynamic CNN (DyCNN) block and a Sequential Self-Attention (SSA) block. The DyCNN block contains a number of residual blocks and an average pooling layer as ResNet (He *et al.*, 2016). To handle targets with different lengths, the pooling layers between the residual blocks are eliminated. Through the DyCNN, a 2D paired distance map $P \in \mathbb{R}^{d \times d}$ is transformed into a feature map $P_c \in \mathbb{R}^{d \times f}$, where f is the number of filters of the residual block. With the SSA block, a weight matrix $A_p \in \mathbb{R}^{r \times d}$ is derived by a two-layer perceptron without bias from P_c:

$$A_p = \text{softmax}(W_{p2} \tanh(W_{p1} P_c^T))$$

where W_{p1} and W_{p2} are learnable parameters. This multilayer perceptron (MLP) block can be regarded as a multi-head attention where the number of neurons r in the last layer is interpreted as the number of attentional heads. The attentional feature map $A_a \in \mathbb{R}^{r \times f}$ is derived by multiplying A_p and P_c, which indicates the relative importance of amino acid sites.
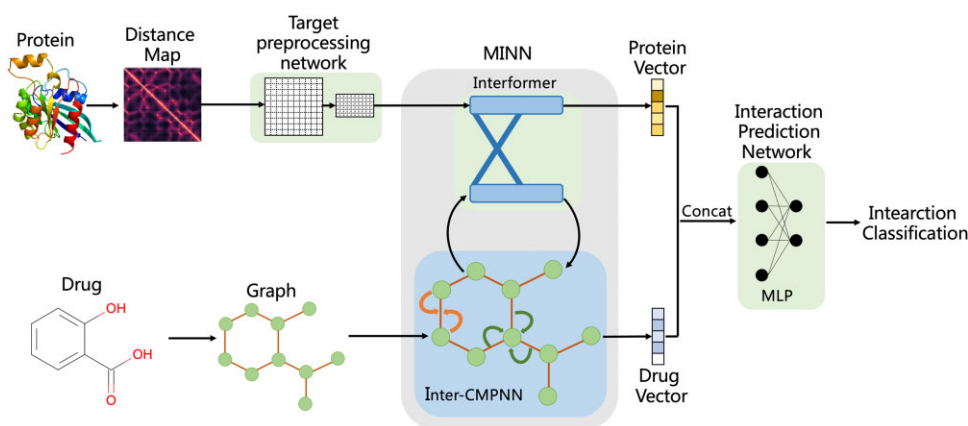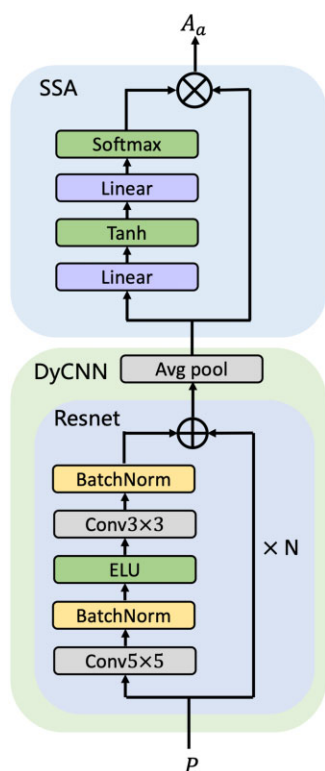
Fig. 1. Architecture of MINN-DTI

Fig. 2. The structure of target preprocessing network

2.3 Mutual interaction neural network (MINN)

The goal of MINN is to learn the representations of targets and drugs while considering their interacting contexts. For this purpose, we design an Interformer module to interact the information extracted from targets and small molecules and an Inter-CMPNN module to support information interacting from the drug side. Thus, we can get more comprehensive representations of the targets and drugs, and consequently boost DTI prediction.

2.3.1 Interformer

Here, we use two interacting transformer decoders to extract feature vectors of targets and drugs, which is called Interformer in short. The structure of Interformer is shown in Figure 3. Each decoder of Interformer consists of one or more identical layers, similar to transformer (Vaswani *et al.*, 2017). Each layer of Interformer consists of three sublayers: a multi-head self-attention layer, an interaction attention layer and a fully connected feed-forward network. The

multi-head self-attention sublayer and the feed-forward sublayer are essentially consistent with transformer, except that the mask operation is eliminated to leverage complete drug and target information following the work of Chen *et al.* (2020).

The interaction attention layer in each decoder of Interformer adopts a multi-head scaled dot attention block to receive the external information from another decoder. The source of external information is the biggest difference between interaction attention layer of Interformer and encode-decoder layer of transformer, where the source of external information is the encoder. A scaled-dot attention block can be expressed as:

$$\text{Attention}(Q, K, V) = \text{softmax}\left(\frac{QK^T}{\sqrt{d_k}}\right)V$$

where Q is the linearly transformed output of the multi head self-attention layer of the decoder, K and V are linearly transformed outputs of the last layer of another transformer decoder, and d_k is the dimension of K and V.

$$\text{head}_i = \text{Attention}(QW_i^Q, KW_i^K, VW_i^V)$$
$$\text{MultiHead}(Q, K, V) = \text{Concat}(\text{head}_1, \dots, \text{head}_h)W^O$$

where W_i^Q, W_i^K, W_i^V and W^O are parameter matrices. With the Interformer, the representation of each small molecule/target is involved with the information of the corresponding interacted target/drug, which conforms to the real situation of DTI.

2.3.2 Inter-CMPNN

The Inter-CMPNN module is implemented by an improved CMPNN, which is a variant of message passing neural network based on directed graph (Song *et al.*, 2020). CMPNN strengthens the message interaction between nodes and edges through three well designed modules (AGGREGATE, COMMUNICATE, UPDATE) for L iterations:

$$m^k(v) = \text{AGGREGATE}(h^{k-1}(e))$$
$$h^k(v) = \text{COMMUNICATE}(m^k, h^{k-1}(v))$$
$$h^k(e) = \text{UPDATE}(h^k(v), h^0(e), h^{k-1}(e)), k = 1, 2, \dots, L$$

where $m^k(v)$ is the message obtained by node v in iteration k, $h^k(v)$ is the hidden representation of node v in iteration k, $h^k(e)$ is the hidden representation of edge e in iteration k. After L iterations, one more iteration is executed to exchange information more thoroughly:

$$m = \text{AGGREGATE}(h^L(e))$$
$$h = \text{COMMUNICATE}(m, h^L(v), x)$$

where x is the raw features of atoms. The AGGREGATE module incorporates a message booster, which processes the information of edges with a maximum pooling layer and calculates the
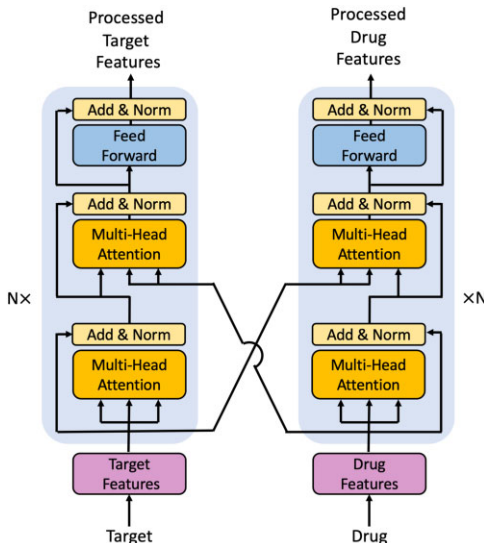
Fig. 3. The structure of Interformer

Fig. 4. Message interaction between Interformer and Inter-CMPNN

element-wise product of the maximum pooling layer's result and the sum of the hidden representations of edges. The UPDATE module is a single-layer neural network with a skip connection, and the COMMUNICATE module takes the form of a multilayer perception.

Here, an Interformer is adopted after the COMMUNICATE function to completely exploit the mutual impacts between targets and drug molecules:

$$m^k(v) = \text{AGGREGATE}(h^{k-1}(e))$$
$$h^k(v) = \text{COMMUNICATE}(m^k, h^{k-1}(v))$$
$$h^k(v), A_a^k = \text{INTERFORMER}(h^k(v), A_a^{k-1})$$
$$h^k(e) = \text{UPDATE}(h^k(v), h^0(e), h^{k-1}(e)), k = 1, 2, \ldots, L$$

where A_a^k is the target feature map in iteration k. Similarly, one more iteration is executed:

$$m = \text{AGGREGATE}(h^L(e))$$
$$h = \text{COMMUNICATE}(m, h^L(v), x)$$
$$h', A_a^o = \text{INTERFORMER}(h, A_a^k)$$

where h' and A_a^o is the final drug graph feature and target feature map. The schematic diagram of message interaction between Interformer and Inter-CMPNN is shown in Figure 4. The last hidden atom representations of each molecular graph and the feature map vectors of each target are averaged to obtain fix-sized vectors of the target and the small molecule, which are then fed to the interaction prediction network.

2.4 Interaction prediction network (IPN)

The obtained target feature vector T and small molecule feature vector D are concatenated and fed to a two-layer perceptron without bias to obtain the prediction result:

$$R = \text{sigmoid}(W_{l2} \, \text{relu}(W_{l1} \text{concat}(T, D)))$$

where W_{l1} and W_{l2} are learnable weight parameters. Since the prediction of DTI is regarded as a binary classification problem, cross entropy is used as the loss function to train the model.

3 Experiments and results

3.1 Datasets

We evaluated our model MINN-DTI and compared it with state-of-the-art DTI prediction methods on three widely used public datasets, human dataset, DUD-E dataset and BindingDB dataset.
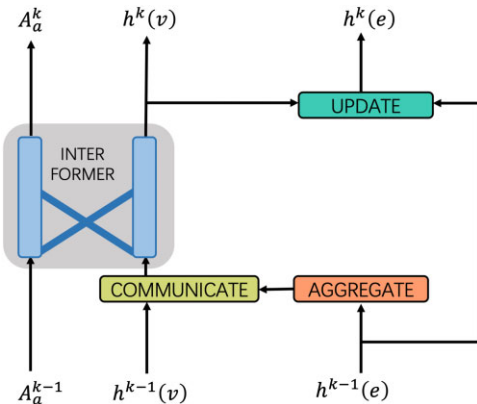
3.1.1 The DUD-E dataset

The DUD-E dataset consists of 22 886 active compounds against 102 targets. For each active compound, 50 decoys are generated, which have similar physico-chemical properties but dissimilar 2-D topologies to the active compound (Mysinger *et al.*, 2012). We processed the DUD-E dataset following the works of Zheng *et al.* (2020) and Ragoza *et al.* (2017), we obtained 22 645 positive examples and 1 407 145 negative examples, which were split according to a three-fold cross-validation strategy. Ligands for the targets belonging to the same target family are put into the same fold. We randomly selected the same number of negative samples as the active samples in training to obtain a balanced model, but we used unbalanced data in model evaluation.

3.1.2 The human dataset

The human dataset contains highly credible positive and negative CPI samples extracted by a systematic screening framework according to a similarity rule (Liu *et al.*, 2015). Following the works of Zheng *et al.* (2020) and Tsubaki *et al.* (2019), we used a dataset with equal number of positive and negative samples, forming 3369 positive interactions between 1052 unique compounds and 852 unique targets. Then, the dataset was randomly divided into a training set, a validation set and a test set according to the ratio of 8:1:1. To evaluate the generalization power of our model on different data, we redivided the human dataset according to molecular scaffold similarities between drugs. The scaffold-based split method implemented in the open source DeepChem package of MoleculeNet (Wu *et al.*, 2018) was used to divide structurally different molecules into training/validation/test sets according to the ratio of 8:1:1.

3.1.3 The BindingDB dataset

The BindingDB dataset (Gao *et al.*, 2018) was a customized subset of the Binding database (Gilson *et al.*, 2016), which is a publicly accessible database that mainly contains the interaction affinities between targets and drug-like small molecules. The BindingDB dataset contains 39 747 positive samples and 31 218 negative samples, which was divided into a large training set (50 155 samples), a validation set (5607 samples) and a test set (5508 samples). To evaluate the generalization power of our model on novel targets, the data of the test set were divided into two parts to check the model performance according to whether the targets appear in the training set.

3.2 Implementation details and experimental settings

We implemented MINN-DTI with Pytorch 1.7.1 (Paszke *et al.*, 2019). The Adam optimizer was used in training and the learning rate was set to 0.0001 (Kingma and Ba, 2015). The number of residual blocks, the number of filters and the dimension of molecular graph features were set to 32. We explored hyperparameters on the human dataset, and the best parameters are listed in Table 1.

Following the work of Zheng *et al.* (2020), hyperparameter optimization was not performed for the DUD-E and BindingDB datasets. All experiments were conducted on NVIDIA RTX3090 GPUs.

3.3 Performance metrics

Here, different metrics were used on different datasets following previous works (Chen *et al.*, 2020; Zheng *et al.*, 2020). The area under the receiver operating characteristic curve (AUC) was used as the main metric to evaluate our model. Besides, the ROC enrichment metric (RE) that describes the ratio of the true positive rate (TPR) to the false positive rate (FPR) at a given FPR threshold was used for performance assessment on the DUD-E dataset, where FPR was set to 0.5%, 1%, 2% and 5%, respectively as the threshold. Moreover, recall and precision were used for performance evaluation on the human dataset, while the area under precision recall curve (PRC) was applied to performance evaluation on the BindingDB dataset. We repeated each experiment three times with different seeds to calculate the mean and the standard deviation as in the work of Zheng *et al.* (2020).

3.4 Results

3.4.1 Performance on the DUD-E dataset

Here, we compared our model with different types of existing methods on DUD-E. These compared methods include two traditional machine learning-based methods NNscore (Durrant and McCammon, 2011) and RF-score (Ballester and Mitchell, 2010), a docking-based method Vina (Trott and Olson, 2009) and three recent deep learning-based methods 3D-CNN (Ragoza *et al.*, 2017), PocketGCN (Torng and Altman, 2019) and DrugVQA (Zheng *et al.*, 2020). As shown in Table 2, MINN-DTI has significant advantage in terms of AUC and RE. The AUC of MINN-DTI is about 2.5% higher than that of the state-of-the-art method DrugVQA, and over 10% higher than that of the other methods. In terms of RE, MINN-DTI is at least twice as high as all the other methods. These results show that our method is more effective in drug screening, since the number of positive samples in DUD-E is much less than that of negative samples, which is close to the actual situation of virtual screening. In addition, deep learning-based methods are obviously superior to the descriptor-based traditional machine learning methods and the docking-based method in terms of AUC and RE,

which suggests that deep learning-based methods are more effective in learning the representations of drugs and targets.

3.4.2 Performance on the human dataset

Here, we compared our method with nine existing methods on the human dataset to further evaluate our model, including k-nearest neighbor (k-NN), random forest (RF), L2-logistic (L2), support vector machine (SVM), graph neural network (GNN) (Tsubaki *et al.*, 2019), graph convolution network (GCN), GraphDTA (Nguyen *et al.*, 2021), TransformerCPI (Chen *et al.*, 2020) and DrugVQA (Zheng *et al.*, 2020). The results are presented in Table 3, from which we can see that our model is 0.2% better than the state-of-the-art method DrugVQA in AUC. However, in terms of recall and precision, SVM is the best. Actually, it is difficult to objectively and completely evaluate the performance of a model by using only recall and precision, as the performance of SVM is generally inferior to deep learning models according to many existing works. Given the reliability of AUC, we can still claim that our method is the best one.

A newly constructed dataset with a scaffold-based split was also used to train and test the above-mentioned methods. As shown in Table 4, our model consistently exceeds all the competitors in AUC. Compared to the results on the random splitting human dataset, the performance of all models on the scaffold splitting human dataset degrades. However, our model has the slightest drop in AUC, i.e. 1.4%, about half of that of the second-place DrugVQA. These results suggest that more comprehensive extraction of DTI information could help enhance our model's ability to identify novel interactions.

3.4.3 Performance on the BindingDB dataset

We also compared our model with GCN, GNN (Tsubaki *et al.*, 2019), GraphDTA (Nguyen *et al.*, 2021), DrugVQA (Zheng *et al.*, 2020) and TransfomerCPI (Chen *et al.*, 2020) on the BindingDB dataset. As shown in Table 5, our model achieves the highest AUC

Table 1. Hyperparameter setting in MINN-DTI

Hyperparameter	Value
Learning rate	0.0001
Number of residual blocks	32
Number of filters	32
Graph feature size	32
Attention heads	8
Hidden size of Decoder	32
Iterations of message passing	4
Dropout	0.2

Table 3. Performance comparison between our model and existing methods on the random splitting human dataset

Model	AUC	Recall	Precision
k-NN[a]	0.860	0.927	0.798
RF[a]	0.940	0.897	0.861
L2[a]	0.911	0.913	0.861
SVM[b]	0.910	**0.966**	**0.969**
GNN[a]	0.970	0.918	0.923
GCN[b]	0.956 ± 0.004	0.862 ± 0.006	0.928 ± 0.010
GraphDTA[b]	0.960 ± 0.005	0.882 ± 0.040	0.912 ± 0.040
TransformerCPI[b]	0.973 ± 0.002	0.916 ± 0.006	0.925 ± 0.006
DrugVQA[a]	0.979 ± 0.003	0.961 ± 0.002	0.954 ± 0.03
MINN-DTI	**0.981 ± 0.003**	0.945 ± 0.030	0.902 ± 0.045

[a]Means results obtained from the article (Zheng *et al.*, 2020).
[b]Means results obtained from the article (Chen *et al.*, 2020).
Best results of the corresponding experiments were represented in bold.

Table 2. Performance comparison between our model and existing methods on the DUD-E dataset

Model	AUC	0.5% RE	1.0% RE	2.0% RE	5.0% RE
NNscore[a]	0.584	4.166	2.980	2.460	1.891
RF-score[a]	0.622	5.628	4.274	3.499	2.678
Vina[a]	0.716	9.139	7.321	5.811	4.444
3D-CNN[a]	0.868	42.559	26.655	19.363	10.710
PocketGCN[a]	0.886	44.406	29.748	19.408	10.735
DrugVQA[a]	0.972 ± 0.003	88.17 ± 4.88	58.71 ± 2.74	35.06 ± 1.91	17.39 ± 0.94
MINN-DTI	**0.992 ± 0.007**	**175.89 ± 12.02**	**90.77 ± 5.81**	**46.49 ± 2.63**	**19.10 ± 0.71**

Note: The first row, the percentage before RE is the given threshold of FPR. Best results of the corresponding experiments were represented in bold.
[a]Means results obtained from the article (Zheng *et al.*, 2020).

Table 4. Performance comparison between our model and existing methods on the scaffold-based splitting human dataset

Model	AUC	Recall	Precision
k-NN	0.841	0.803	0.892
RF	0.885	0.890	0.832
L2	0.881	0.832	0.827
SVM	0.892	0.857	0.883
GNN	0.921 ± 0.002	0.843 ± 0.004	0.855 ± 0.003
GCN	0.905 ± 0.010	0.823 ± 0.012	0.902 ± 0.008
GraphDTA	0.926 ± 0.008	0.855 ± 0.004	0.898 ± 0.006
TransformerCPI	0.948 ± 0.005	**0.930 ± 0.003**	**0.933 ± 0.005**
DrugVQA	0.952 ± 0.002	0.925 ± 0.004	0.928 ± 0.006
MINN-DTI	**0.967 ± 0.003**	0.922 ± 0.013	0.931 ± 0.021

Best results of the corresponding experiments were represented in bold.

Table 5. Performance comparison between our model and existing methods on the BindingDB dataset

Task	AUC	PRC
GNN	0.909 ± 0.002	0.901 ± 0.005
GCN	0.912 ± 0.003	0.907 ± 0.002
GraphDTA	0.923 ± 0.003	0.916 ± 0.004
DrugVQA	0.936 ± 0.005	0.928 ± 0.007
TransformerCPI	0.950 ± 0.002	0.949 ± 0.005
MINN-DTI	**0.961 ± 0.009**	**0.956 ± 0.002**

Best results of the corresponding experiments were represented in bold.

and PRC, which is in line with our expectation. Although this advantage is not as obvious as that on the DUD-E dataset, considering that AUC has less room to improve at the level of more than 95% on these datasets, such progress is still considerable.

We further investigated the generalization capability of our models on the test subsets with/without training targets, the results are shown in Figure 5. We can see that our model performs better than the other models regardless of whether or not the tested targets are in the training set. Our model achieves an AUC of 0.972 ± 0.008 and a PRC of 0.957 ± 0.002 when test targets are in the training set. While for new targets, our model still maintains an AUC of 0.957 ± 0.009 and a PRC of 0.951 ± 0.002. However, the other methods all show a larger drop of performance than MINN-DTI on the subset without the training targets, which means that the performance gap between MINN-DTI and these methods is widened. These results suggest that the generalization ability of our model on new targets is higher than that of these existing methods.

3.5 Ablation study

We conducted ablation studies on the DUD-E and human datasets to check the effectiveness of different configurations of MINN-DTI. All experiments were repeated three times on the divided datasets used above with different seeds to calculate the mean and the standard deviation. Models with different configurations and their performance are presented in Table 6. The first model concatenates the output vectors of DynCNN and CMPNN and uses MLP to predict DTI. The second model replaces Interformer in MINN-DTI with transformer. There are two possible settings: the encoder of transformer receives the information of protein, the decoder of transformer receives the information of drug, or vice versa. For mimicking and competing with Inter-CMPNN, the first setting was used to extract drug information during each round of message passing with the decoder in second model. For the third model, only an Interformer is deployed behind the whole CMPNN module instead of deploying an Interformer during each round of message passing using multiple Interformer as MINN-DTI. As shown in Table 6,

Table 6. Ablation results on the DUD-E and human datasets

Model	DUD-E	Human
Without Interformer	0.953 ± 0.003	0.967 ± 0.004
Transformer & CMPNN	0.975 ± 0.004	0.971 ± 0.007
Single Interformer	0.978 ± 0.006	0.969 ± 0.005
MINN-DTI	**0.992 ± 0.007**	**0.981 ± 0.003**

Best results of the corresponding experiments were represented in bold.
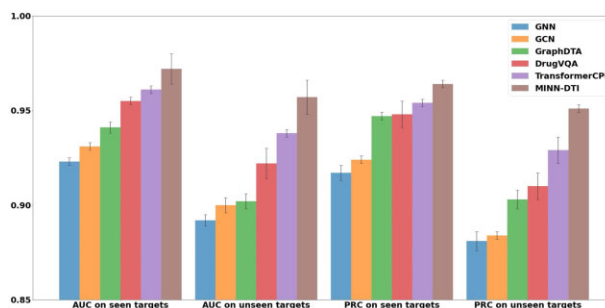

Fig. 5. Performance comparisons on seen and unseen protein targets from the BindingDB dataset. Error bars indicate the standard deviations

MINN-DTI maintains the best performance on both datasets and the model without Interformer module (the first model) performs worst. The performance of the third model is close to the second model, with a difference of only 0.002/0.003 in AUC. However, the results are different on the two datasets. The second model is better than the third model on the human dataset, while the opposite is true on the DUD-E dataset. We speculate that the main reason for the different results may be due to the different data distribution of the two datasets: the test set of DUD-E has unbalanced positive and negative samples, while human dataset is balanced. The second and third models achieve significantly improved performance compared with the first model, which indicates that adopting transformer or Interformer to extract the interaction information between drug and target is helpful for DTI prediction. The second model is still much worse than MINN-DTI, which shows that the Interformer model is more effective than transformer in DTI prediction. As MINN-DTI shows considerable performance advantage over the third model, we believe that the iterative use of Interformer in Inter-CMPNN is beneficial to the extraction of drug and protein interaction information. The ablation results show that MINN-DTI combining Interformer with Inter-CMPNN can indeed improve the prediction performance to a considerable extent.

3.6 Interpretability and visualization

Two representative DTIs were selected to illustrate the interpretability of our model. By inputting the target distance map and the compound graph representations, the model generates multi-head attentions of the target and the compound, and the weights of each amino acid residue and each atom in the target and drug molecule are calculated to identify their importance in the prediction. Protein distance maps and attention bars representing attention weights of residues and ligand atoms are shown in Figure 6. Here, we visualize the top-5 weighted residues of the example target as pink skeletons, and highlight the top-10 weighted atoms by red dots. We found that the significantly weighted residues and atoms are highly consistent with the actual interacting residues and atoms. In CXCR4 protein co-crystal complex 3ODU, GLU288, ASP97 and CYS186 form polar interactions with the drug molecule, and HIS113 and TYR116 form hydrophobic interactions with the drug molecule. These residues and atoms that form the interactions have larger attention weights, which can also be seen in the target ALK5 with co-crystal 3HMM. Meanwhile, there are also residues or atoms with low
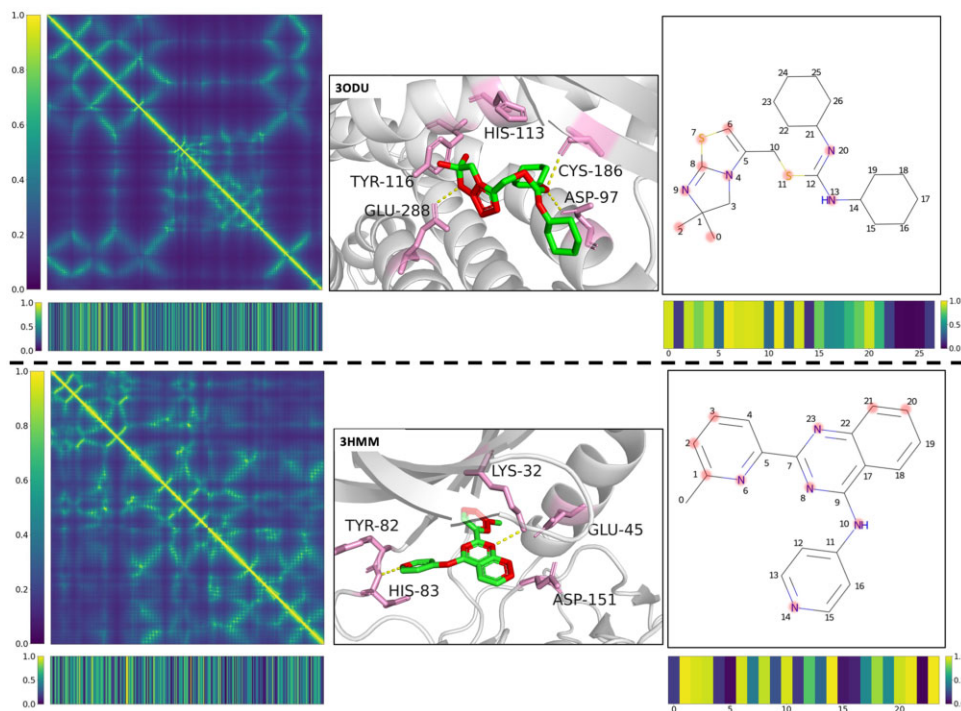
Fig. 6. Attention visualization of DTIs. *Left*: Protein distance maps are displayed in the form of heat maps. The corresponding targets' attention bars are shown. *Middle:* Ligands and predicted important residues are represented as green and pink skeletons, respectively. Predicted important atoms of ligands are highlighted in red. Known hydrogen bonds are marked with yellow dashed lines. Local target structures are painted grey as the background. *Right*: Ligands are represented by 2D Kekule formula. The corresponding predicted important atoms are highlighted by light red dots. Ligands' attention bars are shown (A color version of this figure appears in the online version of this article.)

weight, which are considered to have low contribution to the formation of interactions. For example, in the drug attention bar of complex 3ODU, atoms 21–26 of ligand have small weights, and this group is actually exposed to the solvent without participating in the formation of interaction. The above exploration shows that our model can learn and highlight the important target amino acid residues and drug atoms. This helps us to understand DTIs more comprehensively, which is beneficial to the study on the structure-activity relationship and action mechanism of drugs.

4 Conclusion

In this article, we proposed a novel model MINN-DTI to boost DTI prediction by comprehensively mining the mutual impacts between the targets and drugs, which are represented by protein distance maps and molecular graphs, respectively. To this end, a MINN was designed by combining a newly designed Interformer with an improved CMPNN (called Inter-CMPNN) to capture the interacting context of drugs and targets. Compared with the existing models, MINN-DTI achieves the best performance on three public datasets, due to the fact that MINN-DTI can more effectively exploit the interacting information between targets and drugs. We believe that the Interformer and Inter-CMPNN-based MINN should be also effective in other related tasks, including target–target, target–peptide and drug–drug interaction prediction.

Funding

Reference

Bagherian,M. *et al.* (2021) Machine learning approaches and databases for prediction of drug–target interaction: a survey paper. *Brief Bioinform.*, **22**, 247–269.

Ballester,P.J. and Mitchell,J.B. (2010) A machine learning approach to predicting protein-ligand binding affinity with applications to molecular docking. *Bioinformatics*, **26**, 1169–1175.

Bleakley,K. and Yamanishi,Y. (2009) Supervised prediction of drug–target interactions using bipartite local models. *Bioinformatics*, **25**, 2397–2403.

Chen,L. *et al.* (2020) TransformerCPI: improving compound-protein interaction prediction by sequence-based deep learning with self-attention mechanism and label reversal experiments. *Bioinformatics*, **36**, 4406–4414.

Chen,W. *et al.* (2021) Predicting drug–target interactions with deep-embedding learning of graphs and sequences. *J. Phys. Chem. A*, **125**, 5633–5642.

Durrant,J.D. and McCammon,J.A. (2011) NNScore 2.0: a neural-network receptor–ligand scoring function. *J. Chem. Inf. Model.*, **51**, 2897–2903.

Gao,K.Y. *et al.* (2018) Interpretable drug target prediction using neural representation. In: *Proceedings of the Twenty-Seventh International Joint Conference on Artificial Intelligence (IJCAI-18), Stockholm, Sweden*, pp. 3371–3377.

Gilmer,J. *et al.* (2017) Neural message passing for quantum chemistry. *Proc. Mach. Learn. Res.*, **70**, 1263–1272.

Gilson,M.K. *et al.* (2016) BindingDB in 2015: a public database for medicinal chemistry, computational chemistry and systems pharmacology. *Nucleic Acids Res.*, **44**, D1045–1053.

He,K. *et al.* (2016) Deep residual learning for image recognition. In: *Proceedings of the IEEE Conference on Computer Vision and Pattern Recognition, Las Vegas, Nevada*. pp. 770–778.

Johnson,K.A. (2008) Role of induced fit in enzyme specificity: a molecular forward/reverse switch. *J. Biol. Chem.*, **283**, 26297–26301.

Karimi,M. *et al.* (2019) DeepAffinity: interpretable deep learning of compound-protein affinity through unified recurrent and convolutional neural networks. *Bioinformatics*, **35**, 3329–3338.

Kingma,D.P. and and Ba,J. (2015) Adam: a method for stochastic optimization. In: *Proceedings of the 3rd International Conference on Learning Representations (ICLR 2015), San Diego, CA.*

Lee,I. *et al.* (2019) DeepConv-DTI: prediction of drug–target interactions via deep learning with convolution on protein sequences. *PLoS Comput. Biol.*, **15**, e1007129.

Lenselink,E.B. *et al.* (2017) Beyond the hype: deep neural networks outperform established methods using a ChEMBL bioactivity benchmark set. *J. Cheminform.*, **9**, 45.

Liu,H. *et al.* (2015) Improving compound-protein interaction prediction by building up highly credible negative samples. *Bioinformatics*, **31**, i221–229.

Liu,H. *et al.* (2020) HNet-DNN: inferring new drug–disease associations with deep neural network based on heterogeneous network features. *J. Chem. Inf. Model.*, **60**, 2367–2376.

Mysinger,M.M. *et al.* (2012) Directory of useful decoys, enhanced (DUD-E): better ligands and decoys for better benchmarking. *J. Med. Chem.*, **55**, 6582–6594.

Nguyen,T. *et al.* (2021) GraphDTA: predicting drug–target binding affinity with graph neural networks. *Bioinformatics*, **37**, 1140–1147.

Ozturk,H. *et al.* (2018) DeepDTA: deep drug–target binding affinity prediction. *Bioinformatics*, **34**, i821–i829.

Paszke,A. *et al.* (2019) PyTorch: an imperative style, high-performance deep learning library. *Adv. Neural Inf. Process. Syst. (Nips 2019)*, **32**, 8026–8037.

Peng,Y. *et al.* (2020) TOP: a deep mixture representation learning method for boosting molecular toxicity prediction. *Methods*, **179**, 55–64.

Ragoza,M. *et al.* (2017) Protein–ligand scoring with convolutional neural networks. *J. Chem. Inf. Model.*, **57**, 942–957.

Rifaioglu,A.S. *et al.* (2020) DEEPScreen: high performance drug–target interaction prediction with convolutional neural networks using 2-D structural compound representations. *Chem Sci.*, **11**, 2531–2557.

Rifaioglu,A.S. *et al.* (2021) MDeePred: novel multi-channel protein featurization for deep learning-based binding affinity prediction in drug discovery. *Bioinformatics*, **37**, 693–704.

Skolnick,J. *et al.* (1997) MONSSTER: a method for folding globular proteins with a small number of distance restraints. *J. Mol. Biol.*, **265**, 217–241.

Song,Y. *et al.* (2020) Communicative representation learning on attributed molecular graphs. In: *Proceedings of the 29th International Joint Conference on Artificial Intelligence (IJCAI 2020), Yokohama, Japan*, pp. 2831–2838.

Su,M. *et al.* (2019) Comparative assessment of scoring functions: the CASF-2016 update. *J. Chem. Inf. Model.*, **59**, 895–913.

Tian,K. *et al.* (2016) Boosting compound–protein interaction prediction by deep learning. *Methods*, **110**, 64–72.

Torng,W. and Altman,R.B. (2019) Graph convolutional neural networks for predicting drug–target interactions. *J. Chem. Inf. Model.*, **59**, 4131–4149.

Trott,O. and Olson,A.J. (2010) AutoDock Vina: improving the speed and accuracy of docking with a new scoring function, efficient optimization, and multithreading. *J. Comput. Chem*, **31**, 455–461.

Tsubaki,M. *et al.* (2019) Compound–protein interaction prediction with end-to-end learning of neural networks for graphs and sequences. *Bioinformatics*, **35**, 309–318.

Vaswani,A. *et al.* (2017) Attention is all you need. In: *Proceedings of 31st Conference on Neural Information Processing Systems (NIPS 2017), Long Beach, CA, USA.*

Wallach,I. *et al.* (2015) AtomNet: a deep convolutional neural network for bioactivity prediction in structure-based drug discovery. *arXiv preprint arXiv:1510.02855.*

Wang,X. *et al.* (2021) CSConv2d: a 2-D structural convolution neural network with a channel and spatial attention mechanism for protein–ligand binding affinity prediction. *Biomolecules*, **11**, 643.

Wu,Z. *et al.* (2018) MoleculeNet: a benchmark for molecular machine learning. *Chem. Sci.*, **9**, 513–530.

Xiong,Z. *et al.* (2020) Pushing the boundaries of molecular representation for drug discovery with the graph attention mechanism. *J. Med. Chem.*, **63**, 8749–8760.

Yang,K. *et al.* (2019) Analyzing learned molecular representations for property prediction. *J. Chem. Inf. Model.*, **59**, 3370–3388.

Zhang,Z. *et al.* (2021) FraGAT: a fragment-oriented multi-scale graph attention model for molecular property prediction. *Bioinformatics*, **37**, 2981–2987.

Zheng,S. *et al.* (2019) Identifying structure-property relationships through SMILES syntax analysis with self-attention mechanism. *J. Chem. Inf. Model.*, **59**, 914–923.

Zheng,S. *et al.* (2020) Predicting drug–protein interaction using quasi-visual question answering system. *Nat. Mach. Intell.*, **2**, 134–140.